Autophagy regulates the maturation of hematopoietic precursors in the embryo

Yumin Liu
Key Laboratory of Functional Proteomics of Guangdong Province, Department of Developmental Biology, School of Basic Medical Sciences, Southern Medical University, Guangzhou, China

Linjuan Shi
Key Laboratory of Functional Proteomics of Guangdong Province, Department of Developmental Biology, School of Basic Medical Sciences, Southern Medical University, Guangzhou, China

Yifan Chen
Key Laboratory of Functional Proteomics of Guangdong Province, Department of Developmental Biology, School of Basic Medical Sciences, Southern Medical University, Guangzhou, China

Sifan Luo
Key Laboratory of Functional Proteomics of Guangdong Province, Department of Developmental Biology, School of Basic Medical Sciences, Southern Medical University, Guangzhou, China

Yuehang Chen
Key Laboratory of Functional Proteomics of Guangdong Province, Department of Developmental Biology, School of Basic Medical Sciences, Southern Medical University, Guangzhou, China

Hongtian Chen
Key Laboratory of Functional Proteomics of Guangdong Province, Department of Developmental Biology, School of Basic Medical Sciences, Southern Medical University, Guangzhou, China

Wenlang Lan
Key Laboratory of Functional Proteomics of Guangdong Province, Department of Developmental Biology, School of Basic Medical Sciences, Southern Medical University, Guangzhou, China

Xun Lu
Key Laboratory of Functional Proteomics of Guangdong Province, Department of Developmental Biology, School of Basic Medical Sciences, Southern Medical University, Guangzhou, China

Zhan Cao
Key Laboratory of Functional Proteomics of Guangdong Province, Department of Developmental Biology, School of Basic Medical Sciences, Southern Medical University, Guangzhou, China

Zehua Ye
Key Laboratory of Functional Proteomics of Guangdong Province, Department of Developmental Biology, School of Basic Medical Sciences, Southern Medical University, Guangzhou, China

Jinping Li
Key Laboratory of Functional Proteomics of Guangdong Province, Department of Developmental Biology, School of Basic Medical Sciences, Southern Medical University, Guangzhou, China

Bo Yu
Institute of Hematology, School of Medicine, Jinan University, Guangzhou, China
Elaine Dzierzak
Centre for Inflammation Research, The University of Edinburgh, Edinburgh, UK https://orcid.org/0000-0001-8256-5635
Zhuan Li
zhuanli2018@smu.edu.cn

Key Laboratory of Functional Proteomics of Guangdong Province, Department of Developmental Biology, School of Basic Medical Sciences, Southern Medical University, Guangzhou, China
https://orcid.org/0000-0002-1843-6860

Article

Keywords: autophagy, hematopoietic development, hematopoietic stem cells, endothelial cell to hematopoietic transition, hematopoietic precursors

Posted Date: September 18th, 2023

DOI: https://doi.org/10.21203/rs.3.rs-3288232/v1

Additional Declarations: There is **NO** Competing Interest.

Version of Record: A version of this preprint was published at Nature Communications on March 15th, 2024. See the published version at https://doi.org/10.1038/s41467-024-46453-y.

Abstract

The ability to generate hematopoietic stem cells(HSC) in vitro is advancing as a powerful resource for the treatment of blood diseases. An understanding of the mechanisms regulating HSC development in the embryo would facilitate the achievement of this goal. The aorta-gonad-mesonephros(AGM) region is the site of HSC production in the embryo. As these cells are formed from hemogenic endothelial cells(HEC) and appear as hematopoietic clusters on the lumenal side of the aorta. While several distinct regulators are known to be involved in this process, it is not yet known whether macroautophagy(autophagy) plays a role in hematopoietic development in the pre-liver stage of embryo development. Here, by using the LC3-RFP-EGFP autophagy reporter mouse model, we show that different states of autophagy exist in hematopoietic precursors, and correlate with hematopoietic potential. Deficiency of the autophagy-related gene(Atg) 5 specifically in endothelial cells disrupted endothelial cell to hematopoietic transition(EHT), by blocking the fusion between autophagosome and lysosome. Using combined approaches, including single-cell RNA-sequencing(scRNA-seq), we confirmed that Atg5 deletion interrupted the developmental temporal order of EHT to further affect the pre-HSC I maturation. The rescue experiments with in vivo analyses suggest that autophagy influenced the hemogenic potential of HEC and the formation of pre-HSC I likely via the nucleolin pathway. These findings demonstrate a vital role for autophagy in the formation/maturation of hematopoietic precursors derived from HECs.

Introduction

Hematopoietic stem cells (HSC) are at the apex of the adult hematopoietic hierarchy, providing all mature hematopoietic cells and multipotent progenitor cells. In the embryo, the functional HSCs are generated in the AGM region[1–3] and other sites[4–6]. Functional HSCs derived from hemogenic endothelial cells (HEC)[7–9], undergo developmental processes, some transiting through (pre)HEC, pre-HSC I and pre-HSC II stages[10–15]. Subsequently, HSCs colonize in the fetal liver and migrate into bone marrow[1].

Accumulating data have shown that the production of HSC is regulated by the different transcription factors[15–19], signaling pathways[20–22], closely interacting cells such as macrophages[23–24] and other regulators[1, 25–27]. The continuum of developmental processes from HEC to hematopoietic precursors is described by transcriptome analysis. Bioinformatics approaches have aided in the identification of more surface markers to enrich the cells in these transitions. For example, CD44[11], Procr[28], CD27[29], Ace[10], combined with other basic markers (CD31, CD41, CD45) are able to enrich HECs and hematopoietic precursors. However, our knowledge about the meticulous mechanisms involved in HSC emergence and maturation remains incomplete.

Autophagy is one of the highly conserved intracellular degradation processes involved in maintaining cell survival, cell differentiation, cell death and associated with various diseases[30]. Distinct types of autophagy have been identified, including chaperone-mediated autophagy, microautophagy and macroautophagy, the latter is commonly called autophagy (in this study, we hereafter refer to it as

autophagy)[31]. Autophagy occurs in all cell types responding to environmental stresses, such as deprivation, oxidative stress and thereby maintains cell survival. Autophagy is initiated with the phagophore formation, where cytoplasm and cytoplasmic organelles are enveloped into double-membrane bound as autophagosome, which then migrates to the lysosome forming the autolysosome for degradation[32]. Each step is tightly regulated by the autophagy-related proteins that are initially identified in yeast and have homologs in mammals. The autophagosome formation requires autophagy-related genes (Atg) for activating the evolutionarily conserved ubiquitin-like conjugation. During the fusion process of autophagosome to lysosome, the unconjugated form of Atg8/LC3 (LC3-I) is changed into the lipid form (LC3-II). The early autophagic vacuoles and autolysosomes are able to be distinguished by the elegant transgenic mouse model LC3-RFP-EGFP ($LC3^{R/G}$) based on the distinct pH sensitivities of red fluorescent protein (RFP, pK_a4.5) and enhanced green fluorescent protein (EGFP, pK_a5.9)[33].

Autophagy plays vital roles in the hematopoietic lineage output in adults[30]. Based on the knockout mouse model, Atg5 is involved in the pro-B maturation, T cell survival/proliferation and HSC function[34–36], and Atg7 is as an essential regulator of HSC maintenance and differentiation[37]. Furthermore, the focal adhesion kinase family interacting protein of 200 kDa (Fip200), as a component of ULK-Atg13-Fip200 complex, regulates HSC function, and erythroid/myeloid differentiation in the fetal liver[38]. Recently, transcriptomic data have shown Atg5/7 is highly expressed in the pre-HSCs[39]. However, it is not known whether autophagy regulates HSC development in the earlier embryonic, pre-liver stage, particularly in the first HSC emergence in the AGM region.

In this study, by using Atg5 conditional knockout and autophagy reporter mouse model $LC3^{R/G}$, we examine the regulatory roles of autophagy in hematopoietic development. Our results reveal that Atg5 is essential for the formation/maturation of hematopoietic precursors and HSC function. Based on combined approaches, including single-cell RNA-sequencing data (10x genomics) and rescue experiments, we show that Atg5 deletion interrupted the temporal order of hematopoietic development and affected the maturation of pre-HSCs via nucleolin (Ncl) pathways. These data suggest a role for autophagy in the regulation of HSC development in the embryonic AGM region.

Results

Autophagy is involved in hematopoietic development in the fetal liver and AGM region

The $LC3^{R/G}$ mouse model is used to investigate the dynamics of autophagy in adults[33]. We have checked the expression of GFP and RFP in the HSCs of adult bone marrow (Figure S1A), which is similar to the recent report[40]. Inconsistently, we found that the pattern of RFP and GFP expression appeared differently in the fetal liver (Figure S1B), the RFP signals were weaker compared to GFP signals. Autophagic status

(RFP$^+$GFP$^+$ represents autophagosome before fusion with autolysosome and RFP^{low}GFP^{low} represents autolysosome and RFP$^-$GFP$^-$ represents no autophagic activity) was distinguished based on the fluorescence level of RFP and GFP (Fig. 1A and Figure S1B). In the E12.5 LC3$^{R/G}$ fetal liver, about 80% HSCs (Lin$^-$Sca1$^+$Mac1^{low}CD201$^+$, HSC) and hematopoietic stem/progenitor cells (HS/PC, Lin$^-$Sca1$^+$Mac1^{low}, LSM) were RFP$^+$GFP$^+$, much higher than that in the Lin$^-$ cells and verified by the opposite trend of RFP^{low}GFP^{low} cells and RFP$^-$GFP$^-$ cells(Fig. 1B-1D). Meanwhile, similar trends were found by only analysis of GFP fluorescence signals (Figure S1C-1D), implying the existence of distinct autophagic statuses is related to stemness/differentiation of HS/PC in the fetal liver.

Hematopoietic clusters are emerged from HECs and include pre-HSC I (I Pre, CD31$^+$CD41^{low}CD45$^-$) and pre-HSC II (II Pre, CD31$^+$CD45$^+$). In the E11.5 AGM region, ~ 57% of pre-HSC I were RFP$^+$GFP$^+$, which was significantly higher than the percentage in endothelial cells (CD31$^+$CD45$^-$CD41$^-$, EC) and pre-HSC II (26.6%±2.2% and 34.5%±2.3%, respectively), and then the trend was in contrast to the percentage of RFP^{low}GFP^{low} cells, consistent to the detection of GFP$^+$ cells(Fig. 1A, 1F-1G and Figure S1E-1F). A quite low percentage of RFP$^-$GFP$^-$ cells were found in the pre-HSC I, much lower than that in the EC fraction and pre-HSC II(Fig. 1H). To study the specificity of LC3$^{R/G}$ for labeling autophagy status, immunostaining between GFP/RFP and p62/ Lamp1 was performed. GFP, RFP, and p62 were colocalization in the EC and pre-HSC I and pre-HSC II (presenting autophagosome), and Lamp1 was mainly co-localized with RFP, but not with GFP (presenting autolysosomes, Figure S1G-1H), consistent with the previous report[41]. The geometric mean fluorescence intensity (GeoMFI) of GFP was highest in pre-HSC I compared to that in EC and pre-HSC II fractions, whilst RFP GeoMFI was lowest in the EC fractions of LC3$^{R/G}$ AGM region. Expectedly, the highest GeoMFI ratios of GRP/RFP were in the pre-HSC I, in line with the trend of RFP$^+$GFP$^+$ cells and GFP$^+$ cell percentage (Fig. 1F and Figure S1I-1J), indicating the alteration of autophagy status.

To further investigate the potential of hematopoietic-related cells in different autophagic statuses, RFP$^+$GFP$^+$ and RFP$^{low/-}$GFP$^{low/-}$ cell fractions were cultured in the methylcellulose(because few RFP$^-$GFP$^-$ cells were obtained, cultures were performed by combined RFP^{low}GFP^{low} and RFP$^-$GFP$^-$ cells). Colony-forming unit cultures (CFU-C, including CFU-GEMM, CFU-GM, BFU-E, and CFU-E) were enriched in the RFP$^+$GFP$^+$ fractions, with a higher number of total CFU-Cs and CFU-GM, compared with RFP$^{low/-}$GFP$^{low/-}$ group (Figure S1K). Then, RFP$^+$GFP$^+$ and RFP$^{low/-}$GFP$^{low/-}$ cells were cocultured with OP9-DL1. The number of CD45$^+$ cells derived from RFP$^+$GFP$^+$ pre-HSC I and pre-HSC II was much higher than that from RFP$^{low/-}$GFP$^{low/-}$ groups, but not in the EC fractions (Fig. 1I-1K), suggesting that the maturation of hematopoietic precursors (pre-HSC I and pre-HSC II) are relevant to the earlier autophagic process.

Explant culture is useful for studying hematopoietic precursor development. To check whether autophagy affects hematopoiesis, 3-methyladenine (3-MA, one of autophagy inhibitors)[30] was added in the AGM explant (AGM^{ex}) cultures. Inhibition of autophagy resulted in the significant decline of total colony-forming unit culture (CFU-C) number (including CFU-GEMM, CFU-GM, BFU-E, and CFU-E) from E10.5-E11.5

AGM^{ex}, with the decrease of CFU-GM and BFU-E (Figure S1L). Furthermore, 3-MA treatment reduced the percentage of pre-HSC II, but not of EC and pre-HSC I in E11.5 AGM^{ex}. Meanwhile, the absolute numbers of EC, pre-HSC I and II were reduced dramatically (Figure S1M-1N). These ex vivo data demonstrate the involvement of autophagy in hematopoietic precursor development.

Atg5 regulates HS/PC function in the embryo

Autophagy-related genes regulate HSC maintenance and differentiation[34, 36, 38]. Since Atg5 is the key regulator of autophagy, to test the function of Atg5 in hematopoiesis in the embryo, we generated Vec-Cre;Atg5$^{fl/fl}$ (KO) and control embryos (Atg5$^{fl/fl}$ or Atg5$^{fl/+}$, Ctr). Methylcellulose cultures revealed that Atg5 deletion results in a 38% reduction in CFU-C number per E12.5 fetal liver, with the decrease mainly in CFU-E. Also, CFU-C frequency from the same input cells (1000 cells) was reduced significantly, indicating autophagy is involved in mediating the development of HPC (Fig. 2A-2B), in line with a previous report[38]. Flow cytometric analysis of E12.5 fetal liver cell subsets showed the percentage of LSM was increased, whereas the frequency of Lin$^-$ cell and HSC was unchanged (Fig. 2C-2E). Meanwhile, OP9 cocultures showed that hematopoietic cell (CD45$^+$ cell) number derived from KO FL HSCs was unchanged compared with control group. However, the obvious reduction of hematopoietic cells was found from the same input HSCs, with a decrease of erythroid and lymphoid differentiation ability and altered lineage output (Figure S2A-2F), implicating a possible role for autophagy in hematopoiesis.

Therefore, to investigate the role of autophagy in HSC emergence, distinct stages of AGM regions were analyzed. The percentages and numbers of CD45$^-$CD41$^+$ cells failed to change from E9.5-E11.5 KO AGM region compared to control. Furthermore, the frequency and the number of CD45$^+$CD41$^-$ cells were reduced remarkably only in the E11.5 KO AGM region, but not in the E9.5-E10.5 (Figure S2G-2R). Meanwhile, the deficiency of Atg5 induced a significant decrease in CFU-C in the E10.5-E11.5 AGM region with the reduction of CFU-GM. This was similar at E9.5 (Fig. 2F-2H) and indicates that autophagy influences HPC development in the AGM region.

To check whether Atg5 influences HSC function, cells from KO and control E11.5 AGMs (CD45.2/2) were injected into irradiated recipients (CD45.1/1) and the chimerism of donor cells was examined at 4 and 12–16 weeks post-injection. At 4 weeks, 3 out of 6 recipients were engrafted in the control group. In the Atg5 deficient AGM group, the chimerism of the 3 recipients was less than 5%. After 12–16 weeks transplantation, the chimerism in the Atg5 deficient AGM recipients was 4.08 ± 1.14% compared with control transplant recipients with the chimerism of 22.92 ± 12.65% (Fig. 2I-2J). These data show the critical function of autophagy in the HS/PC function in the AGM region.

The formation/maturation of hematopoietic precursors is altered in the Atg5 deficient AGM region

The regulation of autophagy on hematopoietic precursors was further examined in E10.5-E11.5 AGM cells. At the E10.5, the percentage of pre-HSC I was boosted approximately one-fold after Atg5 deletion (1.20 ± 0.3‰ vs 0.61 ± 0.1‰), whilst the number was increased around 60% (137 ± 23 vs 86 ± 13

cells/embryo equivalent, ee). EC and pre-HSC II cells were not changed. One day later, the alteration of pre-HSC I disappeared. However, the development of pre-HSC II was influenced, with the significant reduction in the percentage (0.19 ± 0.016% vs 0.24 ± 0.004%) and cell number (793 ± 85 vs 1049 ± 81 cells/ee) (Figure S3A-3F) and the hemogenic potential of ECs was reduced, whilst the hematopoietic ability of pre-HSC II was increased (Figure S3G-3H), suggesting the dynamic effects of autophagy on the formation/maturation of hematopoietic cells.

In the E11.5 KO AGM region, the percentage of phenotypic hematopoietic cluster cells ($CD31^+cKit^+$) was increased, but the total number was comparable (Fig. 3A-3B). More surface markers were added to further enrich EC^{plus} ($CD31^+CD45^-CD41^-CD44^+DLL4^+CD201^+cKit^+$), pre-HSC I^{plus} ($CD31^+CD45^-CD41^{low}CD201^+cKit^+$) and pre-HSC II^{plus}($CD31^+CD45^+CD201^+cKit^+$). No alterations were found in the EC^{plus} and pre-HSC I^{plus}, in line with that in the EC and pre-HSC I. The percentage and cell number of pre-HSC II^{plus} was increased around 60% and 44% in the KO AGM region compared to control, in contrast to the trend of pre-HSC II (Fig. 3C-3H and Figure S3F). Expectedly, the frequency and the number of pre-HSC II^{minus} (pre-HSC II without pre-HSC II^{plus}, representing mature hematopoietic cells) was decreased more dramatically (Figure S3I-3J), demonstrating that Atg5 deletion promotes pre-HSC emergence and blocks their maturation.

Immunostaining of CD34, Runx1 and cKit was performed on cryosections from E10.5 control and KO embryos. $CD34^+Runx1^+$ hematopoietic clusters containing 1, 2, 3, 4 or > 5 cells per cluster were quantitated. The number of clusters containing 2 cells per section was significantly higher in the KO aorta than control (Fig. 3I-3K), with the other cluster numbers per section trending to an increase. The number of cells per cluster was enhanced in Atg5-deleted sections (2.0 ± 0.20 vs 1.53 ± 0.17 cells/cluster) (Fig. 3L-3M). The similar trends were found by staining cKit and CD34 (Figure S3K-3M), possibly relative to the changed capacity of recruitment or migration of hematopoietic precursors, as is reported some cells of bigger hematopoietic clusters are recruited from circulation[42]. Altogether, these data suggest that Atg5 regulates the formation / maturation of hematopoietic precursors into functional HS/PCs.

Inhibition of autophagy undermines the fusion of autophagosome-lysosome in hematopoietic precursors

To study whether inhibition of autophagy disrupts the fusion from autophagosome to lysosome, we mated $LC3^{R/G}$-Vec-Cre;$Atg5^{fl/+}$ with $Atg5^{fl/fl}$ to gain $LC3^{R/G}$-Vec-Cre;$Atg5^{fl/fl}$ ($LC3^{R/G}$-KO) embryos. Firstly, the percentage of RFP^+GFP^+ cells was enhanced and that of $RFP^{low}GFP^{low}$ cells was reduced in $LC3^{R/G}$-KO EC, pre-HSC I, pre-HSC II, and hematopoietic clusters ($CD31^+cKit^+$) compare to the corresponding fractions of $LC3^{R/G}$. The reduction of RFP^-GFP^- cells percentage was observed in the EC and hematopoietic clusters(Fig. 4A-4D), indicating that Atg5 conditional deletion impairs the autophagy process of hematopoietic precursors. Secondly, as the GFP fluorescence level is diminished during the process of autophagosome-lysosome fusion, we examined the GeoMFI of GFP and RFP. GeoMFI of GFP

was increased significantly in the RFP^+GFP^+ and $RFP^{low}GFP^{low}$ fractions of EC, pre-HSC I, pre-HSC II, and hematopoietic clusters ($CD31^+cKit^+$) of KO AGM cells as compared with control (Fig. 4E-4L). Although RFP GeoMFI of the total fraction was low, especially in $LC3^{R/G}$ ECs compared with other fractions and GFP GeoMFI was higher in the pre-HSC I as well as the ratios of GFP/RFP, comparable to the RFP^+GFP^+/GFP^+ percentage in the pre-HSC I (Fig. 1F and Figure S1F, S4A-4G). However, the alteration of RFP GeoMFI was not in all fractions and increased only in the RFP^+GFP^+ pre-HSC I cells of $LC3^{R/G}$-KO compared to $LC3^{R/G}$, but not in the other fractions(Fig. 4M-4P, Figure S4H-4K), Additionally, the RFP^+GFP^+ percentage of EC and pre-HSC II were increased in 3-MA treatment AGM region(Figure S4L-4O), with suggestion that Atg5 affects the formation of autolysosome.

As it is reported that autophagy restricts mitochondrial activity[43], we measured mitochondrial mass by the MitoTracker Green (MTG) probe and mitochondrial activity by TMRE. TMRE/MTG GeoMFI ratios were reduced dramatically in the EC, pre-HSC II, but not in the pre-HSC I and hematopoietic cluster ($CD31^+cKit^+$) fractions (Figure S4P-4S), showing that autophagic inhibition leads to the alteration of mitochondrial activity in the AGM region. Altogether, Atg5 deficiency indeed blocks the autophagic process of hematopoietic-related cells to regulate HSC development.

The transcriptomic atlas of control and Atg5-deficient AGM cells

To illustrate the regulatory roles of autophagy in hematopoiesis, we used the droplet-based scRNA-seq (10X Chromium) method to accurately measure the gene expression profiles of individual cells ($7AAD^-Ter119^-$ cells) in the E10.0 AGM (Table S1). 52836 cells passed rigorous quality control with no batch effect. An average of 4383 genes (500–7000) and 21046 transcripts (611-75049) were detected in each individual cell (Figure S5A).

Uniform manifold approximation and projection (UMAP) of all cells separated into 20 clusters by using Seurat software, and included EC (Ramp2, Cdh5), hematopoietic cells (HC, Ptprc, Tyrobp, Fcer1g), megakaryocytes (Mk, Pf4), mesenchymal cells (Mes, Pdgf, Cxcl12), neuron development-related (NPC, Neuron and Schwann cells, Sox2, Ascl1) and epithelial cell (EPC, Epcam) clusters. Hematopoietic-related cells (including EC and HC) were readily distinguished from other cells and the percentage of EC/HC was increased in the Atg5-deleted group compared to control group (Figure S5B-5D). The cell cycle was changed in some KO clusters, such as hematopoietic cells, Mk and mesenchymal cells (Figure S5E), and is consistent with impaired hematopoietic development.

To gain insight into the regulatory mechanism of autophagy on hematopoietic development, the endothelial and hematopoietic cell transcriptomes were further clustered. Nine clusters, including venous EC (C1-C2, vEC: Aplnr, Nrp2), arterial EC (C3, aEC: Gja5, Gja4), HEC (C4, Hlf, Runx1, Gfi1), pre-HSC (C5, Myb, Spn), myeloid progenitor cells (C6, MPC) / macrophages (C7, Mac)(Cybb, Tyrobp), Mk (C8, Gp1bb, Gp5), Erythroid (C9, Gypa, Klf1) were found to be separated. The Mk and erythroid clusters were distant from the other clusters (Fig. 5A and Figure S5F). Cell proportions of vEC and aEC were changed in the KO

group at the cost of Etv2^{+} EC. Consistently, the diameter and area of aorta were decreased in the KO group compared with control (Figure S5G-5I). Atg5-deficiency increased cell proportions of HEC and pre-HSC from selected EC and hematopoietic cell clusters, while the mature hematopoietic cell clusters (C6-C8) were reduced (Fig. 5B). Meanwhile, the alteration of cell cycle phase existed in mature hematopoietic cells and HEC/pre-HSCs (Fig. 5C), implying the possible alteration of EHT and the maturation of hematopoietic cells.

Comparative analyses identify alterations in the developmental process of endothelial to pre-HSC transition after Atg5 depletion

To clearly illustrate the transcriptional changes during EHT, the vEC, aEC and pre-HSC profiles further separated into ten subclusters by known venous/arterial vascular endothelial, hemogenic, and hematopoietic genes, and showed vEC (C1-C4: vEC1-4), arterial EC (C5-C7: aEC1-3), HEC (C8), and pre-HSCs (C9-C10: pre-HSC I and II) (Fig. 5D-5E). Increased endothelial cell proportions existed in the KO subclusters vEC4, aEC1 and aEC3, connecting arterial and venous endothelial cells from the UMAP visualization. Meanwhile, the proportion of HEC was comparable but the percentages of pre-HSC I and II were increased by Atg5 deficiency (Fig. 5D and 5F).

Trajectory analysis by Monocle 2 was performed at single-cell resolution to compare the temporal order of HEC/pre-HSC in the control and KO AGM regions. These data showed that Atg5 deletion led to the accumulation of pre-HSC I and a delay in the developmental process of pre-HSC I relative to the maturation of pre-HSCs (Fig. 5G-5H). RNA velocity analysis estimated the spliced and unspliced gene state, for example, unspliced Runx1 appeared higher in the KO HEC as well as Gfi1, indicating the block of EHT process. Unspliced Kit was higher in the KO pre-HSC I compared to control group, opposite to the trend of Spn (Fig. 5I and Figure S5J-K), suggesting that Atg5 probably promote the process of pre-HSC development by regulating spliced state of Runx1, Gfi1 and Kit. Furthermore, the KEGG signaling pathway analysis showed that pathways related with ubiquitin mediated proteolysis, oxidative phosphorylation were enriched in the control EC and pre-HSCs, whilst p53 signaling pathway and vegf pathway was enriched in the KO pre-HSCs (Figure S5L), indicating the possible signaling pathways of autophagy regulating EHT process.

Atg5 depletion changes the hematopoietic related biological process

To further check the cell components of HEC and pre-HSC during developmental trajectory, the development of HEC in KO group appeared slightly slower than that in the control, but not in the pre-HSC I and pre-HSC II (Fig. 6A-6C). Since we found the EHT process was affected upon Atg5 deletion, HEC and pre-HSC transcriptomic clusters were further analyzed for differentially expressed genes (DEGs) and gene ontology biological process (GOBP, Fig. 6D-6L). Volcano plots showed up / down regulated genes in the KO HECs and the top 15 DEGs were displayed (Fig. 6D and 6E, Table S2). The expression of enriched genes in KO HECs was linked to restricted Smad protein phosphorylation, in agreement with our previous

report[21]. Control HECs showed genes enriched for response to IL-1, autophagosome maturation, positive regulation of ubiquitin transferase activity (which is the main pathway for autolysosome degradation[44]) and mitochondrial fission (Fig. 6F, Table S3), related to the impairment of autolysosome formation and mitochondrial activity after Atg5 ablation.

Volcano plots and bar graphs showed up-regulated genes Ptpn21, Atf5 and down-regulated gene Sox9 in the KO pre-HSC I (Fig. 6G and 6H). GOBP analysis revealed gene enrichment in cell-cell adhesion and vasculogenesis processes in KO pre-HSC I, and enrichment in bone morphogenesis and antigen processing and presentation in control (Fig. 6I). Chemotaxis factors (Ccl3, Cx3cr1) were highly expressed in the control pre-HSC II, and mainly related to leukocyte migration. KO pre-HSC IIs were enriched in the process of nuclear division and angiogenesis (Fig. 6J-6L, Tables S2-S3). These data, together with the results on the increased size of hematopoietic clusters, connect it with the impairment of migration in the KO group.

Atg5 deletion influences the endothelial cell to hematopoietic transition through nucleolin (Ncl) pathway

Cellchat was used to compare the possible communication of all cells via ligand-receptor (L-R) expression. The number and strength of L-R expression/interaction was increased in the KO compared to control (Figure S6A-6B). The Gas pathway was higher in the control, but the opposite trend of most other pathways existed in the KO group, including Grn (granulin), Mdk (midkine), Ptn (pleiotrophin) and Kit (Figure S6C), in line with SCF-dependent pre-HSC production[45]. Since Ncl is the receptor for Mdk and Ptn[46–48], the expression/interactions of Ptn/Mdk-Ncl were enhanced in KO HEC, pre-HSC I and II cells (Fig. 7A), indicating the possible involvement of Ncl in the hematopoiesis.

The expression of *Ptn* and *Mdk* was decreased in the EC of E10.5 KO AGM, but *Ncl* was highly expressed (Figure S6D). Furthermore, immunostaining data showed Ncl with a sheet morphology in the cytoplasm, localized between the nucleus and cell membranes in control EC and pre-HSCs. Ncl fluorescence signals were reduced in KO EC, but not in pre-HSCs and confirmed by fluorescence intensity readings. Interestingly, hubs of Ncl protein signal were observed in the nuclei of KO EC and pre-HSCs, with the number of the larger hubs enhanced significantly after Atg5 deletion (Fig. 7B-7E and Figure S6E), implicating a role for Atg5 in the distribution of Ncl in the cell nucleus and cytoplasm.

As mitochondrial activity was affected in the EC and pre-HSC II by Atg5 deletion, by immunostaining displayed the localization of mitochondrial marker Atp5A and NCL in the EC, pre-HSC I and pre-HSC II single cells. More than 30 single cells were checked and almost all Atp5A signals were localized outside of the nucleus whilst NCL positive signals were in/out of the nucleus, however, double positive localization of NCL + Atp5A was hardly observed, indicating the low possible interaction between mitochondria and NCL (Figure S6F).

AS1411 (Ncl-binding aptamer) is reported to promote the internalization of Ncl[49]. AS1411 was added in the E10.5 AGM^{ex} culture with/without 3-MA. 3-MA reduced the percentages and cell numbers of HEC and pre-HSC I and II, in line with E11.5 AGM^{ex}. Meanwhile, the existence of AS1411 in the 3-MA treatment group enhanced the percentages and cell numbers of HEC and pre-HSC I compared to 3-MA treatment, but not in pre-HSC II (Fig. 7F-7I and Figure S1I-1K, S6G), indicating AS1411 rescues the hematopoietic-related phenotype induced by the inhibition of autophagy. Furthermore, AS1411 failed to rescue the total number of HPC after explant culture, but the potential of BFU-E was recovered partially in the existence of AS1411, even if CFU-GM and CFU-GEMM were not changed (Fig. 7J-7M and Figure S6H). The fluorescence intensity and hubs of NCL were not rescued (Figures S6I-6K). Since the inhibition ability of 3-MA was very strong compared with KO mouse model, we modified the experimental setup. 3-MA treatment occurred one day instead of three days. The stronger rescue roles of AS1411 in the number/percentage of PK44 HEC and pre-HSC I^{plus} were observed, although it still failed to play functions in pre-HSC II^{plus} (Fig. 7N-7Q and Figures S6L). Furthermore, the fluorescence intensity of NCL was rescued compared with 3-MA group, as well as the number of hubs and bigger hubs (Figures S6M). Altogether, these data suggest that autophagy plays key role in the EHT through the Ncl pathway.

Discussion

Here, we have identified that Atg5, an autophagy-related gene, is a key regulator of hematopoietic precursor formation/maturation into mature hematopoietic progenitor/stem cells during embryonic development, through blockage of the fusion of autophagosome with lysosome. Mechanically, Atg5 plays a critical role in endothelial cell to hematopoietic transition by the Ncl pathway.

Autophagy is involved in HS/PC function

Autophagy is a conserved process, involved in HSC maintenance, survival, and differentiation mediated by different Atgs. Atg5 is the one of ‘core’ key autophagy components. Atg5 is required for the development of pro- to pre-B cells and for maintaining the B1-a B cells in the periphery[36]. The lack of Atg5 in hematopoietic cells (via Vav-cre mediated deletion) leads to the impaired reconstitution ability of HSCs[35]. Additionally, Atg7 is essential for adult HSC function[37, 50], but less essential in fetal liver HSC. In the fetal liver, Fip200 influences the number and frequency of HSC[37]. Our data illustrate that deficiency of Atg5 in the endothelial cells resulted in the alteration of lineage output from fetal liver HSC by ex vivo culture system, in line with the roles of Atg5 in bone marrow HSC[51]. Meanwhile, Atg5 depletion reduced the number of hematopoietic progenitor cells (CFU-Cs) and impaired the HSC function by transplantation in the AGM region (pre-liver stage). Therefore, Atg5 plays pivotal roles not only in the fetal liver stage, but also in the earlier stage of hematopoiesis in the embryo, regulating HS/PC development, and thus providing support for a role for autophagy in embryonic hematopoiesis.

The regulation of autophagy in hematopoietic precursors

LC3 (Map1lc3) is a cytosolic protein that, when lipidated, localizes to the surface of autophagosomes as an autophagosome marker. The transgenic mouse model $LC3^{R/G}$, with RFP and EGFP, is used to observe and quantify the status of autophagy in vivo. RFP signal is weaker compared to GFP, which is different from that in the adult bone marrow[40]. Even though RFP^+GFP^+, $RFP^{low}GFP^{low,}$ and RFP^-GFP^- fraction were observed, the RFP signal was not as strong as that in the adult bone marrow since we detected the RFP signals in the bone marrow as control, suggesting the distinct autophagy activity between embryos and adults at steady state. HS/PCs in the fetal liver are mostly LC3-RFP^+GFP^+ compared with that in Lin^-, indicating RFP^+GFP^+ signals are related to the immature states. Meanwhile, in the AGM region, RFP^+GFP^+ signals are higher in the pre-HSC I than that in the pre-HSC II, possibly because pre-HSC II fraction is less enriched and may contain mature myeloid cells. Altogether, the autophagic status varies between the hematopoietic cell fractions.

Atg5 knockout delays the maturation and reduces the survival of adult-generated neurons in the hippocampus[52]. Consistent with neuron development, our data demonstrate that autophagy regulates the maturation of hematopoietic precursors in three aspects. Firstly, our cocultures show that the abilities of maturation in pre-HSC I and II are related to the stage of earlier autophagy (RFP^+GFP^+, not $RFP^{low/-}GFP^{low/-}$), suggesting that RFP^+GFP^+ pre-HSCs represent an immature cell state. Secondly, the percentages and cell numbers of hematopoietic precursors are enhanced in the Atg5 KO AGM region, indicating the blockade of maturation (in vivo data). Lastly, the GFP signal is higher in the hematopoietic precursors of $LC3^{R/G}$-KO AGM, based on the blockade of lysosome formation, suggesting that Atg5 deletion maintains immature hematopoietic precursors. We couldn't exclude the possible contribution of the enhanced pre-HSC I formation, but the maturation of hematopoietic precursors is indeed regulated by autophagy.

Aberrant autophagy also modulates leukemogenesis. The autophagic regulator of the PI3K/AKT/mTOR pathways has been implicated in leukemogenesis[53, 54]. Atg5 plays roles in MLL-AF9 AGM initiation, but not in the secondary transplanted leukemia stem cells[55, 56]. In adults, autophagy maintains HSC function and inhibits senescence via Foxo3a and Bag3-dependent manner[40, 57]. Lysosomes also regulate HSC metabolism and balance the maintenance of HSC quiescence versus activation[58, 59]. Interestingly, our data show that Atg5 deficiency partially blocks the fusion between autophagosome and lysosome in the hematopoietic related cell fractions, such as endothelial cells, and pre-HSCs, particularly in hematopoietic precursors. It likely results in the failure of clearance through the lysosome degradation, which possibly contributes to the increase of cell number in hematopoietic clusters. In agreement with this, the transcriptomic data display biologic processes related to autophagosome maturation and mitochondrial fission/fusion after Atg5 deletion. Recent reports show that mitochondrial membrane potential is a successful approach to separate quiescent HSCs[60]. We have found that the mitochondrial activity(TMRE/MTG, energy metabolism) is decreased in the hematopoietic precursors after Atg5 deletion.

RNA velocity analysis supports that the splicing status of Runx1 and Gfi1 are altered by Atg5 deletion, in line with the key roles of Runx1 and Gfi1 in the EHT process[15, 16, 18]. Recent report has shown the regulation of Myd88-dependent TLR signaling on hematopoietic clusters formation[61], consistently, our KEGG signaling pathway analysis showed the reduced toll like receptor pathways. Except that, the ubiquitin mediated proteolysis pathway was different trend in the EC and pre-HSC II, implying the possible dynamic roles of autophagy in protein degradation during EHT stage. Recent report has displayed the involvement of autophagy in the protein hemostasis in the bone marrow HSPC[40]. Rare number of pre-HSCs restricts to check more accurate autophagic flux states and protein degradation of pre-HSCs in the AGM region. However, it remains to be studied whether other autophagy mechanisms, such as mitophagy regulates hematopoiesis and how autophagy affects the metabolism of mitochondrial, protein hemostasis in the embryo.

Atg5 alters the distribution of Ncl to mediate the hemogenic potential of endothelial cells

Hematopoietic precursor cells bud from hemogenic endothelial cells. Recent research shows that the HECs are derived from specified-arterial endothelial cells[11]. We specifically deleted Atg5 in ECs to investigate the role(s) of autophagy. Our scRNA-seq data shows that the development processes of EC are interrupted, in consistent with the reduced aorta size/area. A recent report demonstrates that autophagy modulates EC junctions by repressing migration of neutrophils[62]. From our bioinformatics analysis, KO HECs are highly enriched in genes restricted to Smad protein phosphorylation, in line with our previous report that smad4 restricts the formation of hematopoietic clusters[21]. Meanwhile, Atg5 deleted pre-HSC I/IIs still sustain the capacity for vascular development, with the impairment of migration. Hence, our data illustrate that autophagy likely affects the acquisition of pre-HSC hematopoietic capacity.

It is reported that the Ncl distribution links with the cell cycle of HSC in the bone marrow[63]. Our transcriptomic data have revealed alterations in the cell cycle in Atg5 deleted EC and pre-HSCs. Ncl transcripts are increased in the KO as compared to control ECs, but the protein level is not enhanced. Interestingly, the distribution of Ncl in the intracellular compartments are affected in the KO EC and pre-HSCs, and is likely affecting the hemogenic potential of HECs and the maturation of pre-HSC. The existence of Ncl binding aptamer (AS1411) partially rescues the number and frequency of HEC and pre-HSC I in explant cultures, confirming that Ncl indeed mediates the regulation of autophagy on the hematopoiesis. However, it appears to be irreversible, as autophagy impairs pre-HSC II development by 3-MA (inhibitor of autophagy), even if only one day 3-MA treatment. Since 3-MA is a pan-inhibitor, it exhibits greater effects on hematopoiesis as compared to the effects of Atg5 deletion, possibly explaining its irreversible effects on hematopoietic cells.

In conclusion, we have found that autophagy plays vital roles in the hematopoietic development, particularly in the maturation of hematopoietic precursors into functional HSC, with the modulation on

the hemogenic potential of HEC and the maturation of pre-HSC I through Ncl pathways, providing a potential regulator for HS/PC regeneration.

Methods

Mouse models

LC3-RFP-EGFP (LC3$^{R/G}$, from Jackson lab.,[33]), VE-cadherin-Cre (from Bing Liu, [64]), Atg5$^{fl/fl}$ (from the RIKEN BioResource Center,[65]) mice were used for timed mating and C57BL/6-Ly5.1/1[66] (8–12 weeks) mice were as transplantation recipients.

Mice were housed in the animal facility of Southern Medical University and mice experiments were approved by the ethics committee of Southern Medical University.

Mouse embryo generation

LC3$^{R/G}$ embryos were generated from LC3$^{R/G}$ male mice crossed with C57BL/6-Ly5.2/2 female mice. Male Vec-Cre;Atg5$^{fl/+}$ mice were crossed with female Atg5$^{fl/fl}$ mice for Atg5 deficient embryos (Ly5.2/2). The embryo stages were identified by counting somite pairs and tails were used for genotyping.

Flow cytometric analysis

Cells from fetal liver and AGM regions were used for flow cytometric analysis. In fetal liver, phenotypic defined HS/PCs (Lin$^-$Sca1$^+$Mac1^{low}) and HSCs (Lin$^-$Sca1$^+$Mac1^{low}CD201$^+$) were analyzed by lineage cocktail (Ter119, Gr1, NK1.1, CD3, B220), Sca1, Mac1 and CD201. In the AGM region, digested cells were stained by antibody combination: CD31, CD41, CD45, CD43, CD44, DLL4, CD201, cKit for HECs and pre-HSCs. 7AAD or Hoechst was used for dead cell exclusion.

Hematopoietic progenitor and stem cell assays

Single-cell suspensions from AGM and fetal liver or cultures were plated in the methylcellulose (M3434; Stem Cell Technologies) for CFU-C assay. The counting and quantification of CFU-C was according to previous report[23]. E11.5 control or KO AGM cells (1-1.5 ee, Ly5.2/2) were co-injected intravenously with supporting cells (2x10^5 leukocytes from bone marrow Ly5.1/1) into 8.5Gy(4.5Gy + 4Gy) irradiated recipient mice(Ly5.1/1). Peripheral blood chimerism assays were performed at 4, 12/16 weeks after transplantation.

Explant cultures and OP9-DL1 cocultures

AGM explant (AGM^{ex}) culture was performed as previously described[2, 3]. In brief, AGMs were deposited on a nylon membrane (Millipore) placed on metallic supports and cultured in MyeloCult M5300 or H5100 (Stem Cell Technologies) supplemented with 10 μM hydrocortisone (Sigma-Aldrich). After 3–4 days culture, explants were collected and dissociated into single cells by 0.125% collagenase digestion (Sigma-Aldrich) for flow cytometry analysis and further culture. In some conditions, 3-methyladenine(3-MA,

Merck, 1mM) and AS1411(5'-GGTGGTGGTGGTTGTGGTGGTGGTGG-3', the aptamer of nucleolin, 10μM, from Ruibiotech) were added into the explant cultures.

Endothelial cells, pre-HSC I and pre-HSC II cells were sorted from AGM region and were co-cultured with OP9-DL1 cells(stem cell factor, 100 ng/mL; IL-3, 100 ng/mL; and Flt3-ligand, 100 ng/mL; PeproTech) or OP9 cells(stem cell factor, 20 ng/mL; IL-7, 10 ng/mL; and Flt3-ligand, 10 ng/mL; PeproTech) for 7 days as previous report[67] and cells were harvested by mechanical pipetting for flow cytometric analysis.

Immunostaining

Immunostaining was performed as described previously[11]. E10.5 embryos were fixed (2% paraformaldehyde/PBS, 20 min, 4°C), equilibrated in 20% sucrose/PBS at 4°C overnight and then embed in the Tissue Tek before freezing. From each WT and KO embryo, we sequenced the sections and chose 4–5 sections per embryo from ~ 100 sections at the similar area along the rostral-caudal axis. After additional blocking of endogenous biotin step, antibodies staining were performed. Primary and secondary antibody were used at the following concentrations: Anti-c-Kit (1:100, BD), biotinylated anti-CD34 (1:200, eBioscience), Runx1 (1:500, Abcam) and Hoechst for nuclear staining. Additionally, Ncl (1:100) was used for staining ECs and pre-HSCs sorted by flow cytometry and spun onto slides. Secondary antibodies: Alexa Flour 647 anti-rat IgG (1:500), AF488 anti-rabbit IgG (1:1000) and Streptavidin Cy3 (1:1000). The image procedures were performed by confocal microscope (Zeiss LSM 880).

Single-cell RNA-sequencing

For droplet-based scRNA-seq (10x genomics), AGM cells were sorted by flow cytometry according to $Ter119^-$ cells or $Ter119^-CD31^+/CD45^+/CD41^+$ cells, and then the latter was mixed with negative cells (Table S1). Libraries were produced with a Chromium system (10×Genomics, PN1000268) following the manufacture's instruction and sequenced on Illumina Novaseq 6000 platform in 150 bp paired-end manner (sequenced by Novogene and Berry Genomics).

Single-cell transcriptome analysis and quality control

Sequencing data from 10x Genomics was processed with the Cell Ranger software for each sample. Raw data in FASTQ format was processed and aligned to the mm10 mouse reference genome (https://cf.10xgenomics.com/supp/cell-exp/refdata-gex-mm10-2020-A.tar.gz) with the Cell Ranger v5.0.1 pipeline(10x Genomics, https://www.10xgenomics.com/). Doublet cells were removed using DoubletFinder R package (v2.0.3)[68] with the recommended doublet rate by the pipeline. Then filter low-quality cells, we retained cells: (1) expressing 500-7,000 genes, (2) less than 10% of reads mapped to mitochondrial genes, and (3) less than 40% of reads mapped to ribosome genes. We sequenced 74,754 single cells, and retained 52,836 cells after the quality-control process of the primary sequencing data.

Batch correction, data integration, dimensionality reduction, cell clustering analysis

R package Seurat (v4.1.0)[69] was used for downstream analysis and visualization. Raw counts were normalized with the “NormalizeData” function. Highly variable genes (HVGs) were selected by using the “FindVariableFeatures” function with default parameters, which were applied for principal-component analysis (PCA), remove batch effects, data integration and cell clustering.

We removed batch effects from different samples at the same developmental stage by canonical correlation analysis which was conducted in Seurat. Data integration was performed with the “FindIntegrationAnchors” function to determine the integration anchors. Then, based on the union of the top 2,000 HVGs of each dataset, we used the “IntegrateData” function to perform the dataset integration.

We took the union of the top 2000 genes with the highest expression and dispersion from both datasets used for PCA. Then the “ScaleData” function was implemented to scale and center the genes in the dataset. Dimension reduction was conducted using the top significant principal components (PCs) and visualized by UMAP. Finally, we used the “FindClusters” function to identify clusters of cells. Marker genes were identified depending on the adjusted p-values < 0.05 (determined by two-sided Wilcoxon rank-sum test and adjusted using Bonferroni correction) (Table S2).

Identification of DEGs and enrichment analysis

DEGs were identified by “FindMarkers” function in Seurat using the Wilcox method. Genes with the absolute value of log2 fold change > 1 and p-value < 0.05 were considered as DEGs (Table S2). And then we sequenced these genes from highest to lowest according to log2 fold change in KO to control. Gene Ontology Biological Process(GOBP) Kyoto Encyclopedia of Genes and Genomes (KEGG) enrichment analyses of these lists was conducted using GSEA (v4.2.3, https://www.gsea-msigdb.org/gsea/index.jsp)[70] (Table S3).

Cell cycle analysis

Cell cycle-related genes set of 43 G1/S genes and 54 G2/M genes were used for cell cycle analysis[71, 72]. We classified the cycling phases using a similar method to Tirosh et al[11, 73]. We assigned a corresponding cell cycle identity to each cell by calculating the average expression of each gene set. Cells with G1/S score < 2 and G2/M score < 2 were assigned as “quiescent”, else as “proliferative”. Among proliferative cells: 1) G2/M score > G1/S score, assigned as “G2/M”, 2) G1/S score > G2/M score and G2/M score < 2, assigned as “G1”, 3) G1/S score > G2/M score and G2/M score ≥ 2, assigned as “S”.

Trajectory analysis

Monocle 2 (version 2.22.0)[74] was used to determine the pseudotime of ten subclusters from vEC, aEC and pre-HSC clusters, and pseudotime was scaled from 0 to 1. Identified significant genes used in pseudotime analysis by the "dispersionTable" function. We followed the official vignette with recommended parameters.

RNA velocity

To predict the direction of EHT from EC, HEC and pre-HSC, we used the velocyto (v0.17.17)[75] with default parameters. Further analysis and visualization were carried out using R package velocyto.R (v0.6).

Cell-cell communication analysis

To identify and visualize the communicating interactions between HEC/pre-HSCs and other cells (excluding EC and HCs) at a single-cell resolution by using R package CellChat (version 1.1.3)[76]. We followed the official workflow to compare the potential ligand-receptor interactions between control and KO groups were obtained.

QUANTIFICATION AND STATISTICAL ANALYSIS

All graphs were generated using GraphPad Prism 8. All data are presented as the mean ± SEM. Student t-test is for comparisons of 2 groups and one-way ANOVA analysis of variance test is for comparisons of > 2 groups. $P < 0.05$ was considered significant. *$p < 0.05$, **$p < 0.01$, ***$p < 0.001$, ****$p < 0.0001$. Further statistical details of experiments can be found in the figure legends. The number of biological replicates is indicated with 'n'.

Declarations

Data and code availability

The raw sequencing data generated in the present study are deposited in the GSA (Genome Sequence Archive in BIG Data Center, Beijing Institute of Genomics, Chinese Academy of Sciences) with the accession number (CRA008812 https://ngdc.cncb.ac.cn/gsa/s/7ep9swyS). The processed datasets generated this study are deposited in the OMIX China National Center for Bioinformation/Beijing Institute of Genomics, Chinese Academy of Sciences), under accession number (OMIX002331 https://ngdc.cncb.ac.cn/omix/preview/M33PPaoZ).

Acknowledgements

The authors thank all lab members for helpful comments. We also thank Wenyue Xu for for the contribution of Atg5 $^{fl/fl}$ and Bing Liu for Vec-Cre mice. We thank Dr. B. Liu and Dr. Y. Lan for critical discussion. The authors thank the Institute of Hematology, Jinan University, for providing flow cytometric sorting. This work was supported by grants from the National Key Research and Development Program (2019YFA0111100, 2019YFA0801802), the National Natural Science Foundation of China (82070105).

Authorship Contributions

Zhuan Li conceived the project and designed the experiments. Yumin Liu, Linjuan Shi, Sifan Luo and Yuehang Chen performed experiments. Yifan Chen mainly performed bioinformatics analysis. Hongtian Chen and Wenlang Lan irradiated mice. Zehua Ye helped for genotyping. Jinping Li helped bioinformatics analysis. Xun Lu, Zhan Cao and Bo Yu helped for FACS. Zhuan Li and Yumin Liu wrote the manuscript and Elaine Dzierzak revised the manuscript.

Declaration of interests

The authors have no financial interests to disclose.

References

1. Dzierzak, E. & Bigas, A. Blood Development: Hematopoietic Stem Cell Dependence and Independence. CELL STEM CELL 22, 639–651 (2018).
2. Medvinsky, A. & Dzierzak, E. Definitive hematopoiesis is autonomously initiated by the AGM region. CELL 86, 897–906 (1996).
3. Muller, A.M., Medvinsky, A., Strouboulis, J., Grosveld, F. & Dzierzak, E. Development of hematopoietic stem cell activity in the mouse embryo. IMMUNITY 1, 291–301 (1994).
4. Gekas, C., Dieterlen-Lièvre, F., Orkin, S.H. & Mikkola, H.K.A. The Placenta Is a Niche for Hematopoietic Stem Cells. DEV CELL 8, 365–375 (2005).
5. Li, Z. *et al.* Mouse Embryonic Head as a Site for Hematopoietic Stem Cell Development. CELL STEM CELL 11, 663–675 (2012).
6. Ottersbach, K. & Dzierzak, E. The Murine Placenta Contains Hematopoietic Stem Cells within the Vascular Labyrinth Region. DEV CELL 8, 377–387 (2005).
7. Boisset, J. *et al.* In vivo imaging of haematopoietic cells emerging from the mouse aortic endothelium. NATURE 464, 116–120 (2010).
8. Kissa, K. & Herbomel, P. Blood stem cells emerge from aortic endothelium by a novel type of cell transition. NATURE 464, 112–115 (2010).
9. Lancrin, C. *et al.* The haemangioblast generates haematopoietic cells through a haemogenic endothelium stage. NATURE 457, 892–895 (2009).
10. Fadlullah, M.Z.H. *et al.* Murine AGM single-cell profiling identifies a continuum of hemogenic endothelium differentiation marked by ACE. BLOOD 139, 343–356 (2022).
11. Hou, S. *et al.* Embryonic endothelial evolution towards first hematopoietic stem cells revealed by single-cell transcriptomic and functional analyses. CELL RES 30, 376–392 (2020).
12. Howell, E.D. & Speck, N.A. Forks in the road to the first hematopoietic stem cells. CELL RES 30, 457–458 (2020).
13. Rybtsov, S. *et al.* Hierarchical organization and early hematopoietic specification of the developing HSC lineage in the AGM region. J EXP MED 208, 1305–1315 (2011).
14. Zeng, Y. *et al.* Tracing the first hematopoietic stem cell generation in human embryo by single-cell RNA sequencing. CELL RES 29, 881–894 (2019).
15. Zhu, Q. *et al.* Developmental trajectory of prehematopoietic stem cell formation from endothelium. BLOOD 136, 845–856 (2020).
16. Chen, M.J., Yokomizo, T., Zeigler, B.M., Dzierzak, E. & Speck, N.A. Runx1 is required for the endothelial to haematopoietic cell transition but not thereafter. NATURE 457, 887–891 (2009).

17. Kaimakis, P. *et al.* Functional and molecular characterization of mouse Gata2-independent hematopoietic progenitors. BLOOD 127, 1426–1437 (2016).
18. Lancrin, C. *et al.* GFI1 and GFI1B control the loss of endothelial identity of hemogenic endothelium during hematopoietic commitment. BLOOD 120, 314–322 (2012).
19. Thambyrajah, R. *et al.* GFI1 proteins orchestrate the emergence of haematopoietic stem cells through recruitment of LSD1. NAT CELL BIOL 18, 21–32 (2016).
20. Crisan, M. *et al.* BMP signalling differentially regulates distinct haematopoietic stem cell types. NAT COMMUN 6, 8040 (2015).
21. Lan, Y. *et al.* Endothelial Smad4 restrains the transition to hematopoietic progenitors via suppression of ERK activation. BLOOD 123, 2161–2171 (2014).
22. McGarvey, A.C. *et al.* A molecular roadmap of the AGM region reveals BMPER as a novel regulator of HSC maturation. J EXP MED 214, 3731–3751 (2017).
23. Li, Z. *et al.* A role for macrophages in hematopoiesis in the embryonic head. BLOOD 134, 1929–1940 (2019).
24. Mariani, S.A. *et al.* Pro-inflammatory Aorta-Associated Macrophages Are Involved in Embryonic Development of Hematopoietic Stem Cells. IMMUNITY 50, 1439–1452 (2019).
25. Wang, F. *et al.* Single-cell architecture and functional requirement of alternative splicing during hematopoietic stem cell formation. SCI ADV 8, g5369 (2022).
26. Yvernogeau, L. *et al.* Multispecies RNA tomography reveals regulators of hematopoietic stem cell birth in the embryonic aorta. BLOOD 136, 831–844 (2020).
27. Zhou, J. *et al.* Combined Single-Cell Profiling of lncRNAs and Functional Screening Reveals that H19 Is Pivotal for Embryonic Hematopoietic Stem Cell Development. CELL STEM CELL 24, 285–298 (2019).
28. Zhou, F. *et al.* Tracing haematopoietic stem cell formation at single-cell resolution. NATURE 533, 487–492 (2016).
29. Li, Y., Gao, L., Hadland, B., Tan, K. & Speck, N.A. CD27 marks murine embryonic hematopoietic stem cells and type II prehematopoietic stem cells. BLOOD 130, 372–376 (2017).
30. Orsini, M., Morceau, F., Dicato, M. & Diederich, M. Autophagy as a pharmacological target in hematopoiesis and hematological disorders. BIOCHEM PHARMACOL 152, 347–361 (2018).
31. Boya, P., Reggiori, F. & Codogno, P. Emerging regulation and functions of autophagy. NAT CELL BIOL 15, 713–720 (2013).
32. Mizushima, N., Yoshimori, T. & Levine, B. Methods in mammalian autophagy research. CELL 140, 313–326 (2010).
33. Li, L., Wang, Z.V., Hill, J.A. & Lin, F. New autophagy reporter mice reveal dynamics of proximal tubular autophagy. J AM SOC NEPHROL 25, 305–315 (2014).
34. Gomez-Puerto, M.C. *et al.* Autophagy Proteins ATG5 and ATG7 Are Essential for the Maintenance of Human CD34(+) Hematopoietic Stem-Progenitor Cells. STEM CELLS 34, 1651–1663 (2016).

35. Jung, H.E., Shim, Y.R., Oh, J.E., Oh, D.S. & Lee, H.K. The autophagy Protein Atg5 Plays a Crucial Role in the Maintenance and Reconstitution Ability of Hematopoietic Stem Cells. IMMUNE NETW 19, e12 (2019).
36. Miller, B.C. *et al.* The autophagy gene ATG5 plays an essential role in B lymphocyte development. AUTOPHAGY 4, 309–314 (2008).
37. Mortensen, M., Watson, A.S. & Simon, A.K. Lack of autophagy in the hematopoietic system leads to loss of hematopoietic stem cell function and dysregulated myeloid proliferation. AUTOPHAGY 7, 1069–1070 (2011).
38. Liu, F. *et al.* FIP200 is required for the cell-autonomous maintenance of fetal hematopoietic stem cells. BLOOD 116, 4806–4814 (2010).
39. Hu, Y. *et al.* Single-cell RNA sequencing highlights transcription activity of autophagy-related genes during hematopoietic stem cell formation in mouse embryos. AUTOPHAGY 13, 770–771 (2017).
40. Chua, B.A. *et al.* Hematopoietic stem cells preferentially traffic misfolded proteins to aggresomes and depend on aggrephagy to maintain protein homeostasis. CELL STEM CELL 30, 460–472 (2023).
41. Kaminskyy, V., Abdi, A. & Zhivotovsky, B. A quantitative assay for the monitoring of autophagosome accumulation in different phases of the cell cycle. AUTOPHAGY 7, 83–90 (2011).
42. Porcheri, C. *et al.* Notch ligand Dll4 impairs cell recruitment to aortic clusters and limits blood stem cell generation. EMBO J 39, e104270 (2020).
43. Papa, L., Djedaini, M. & Hoffman, R. Mitochondrial Role in Stemness and Differentiation of Hematopoietic Stem Cells. *STEM CELLS INT* 2019, 4067162 (2019).
44. Shi, C.S. *et al.* Activation of autophagy by inflammatory signals limits IL-1beta production by targeting ubiquitinated inflammasomes for destruction. NAT IMMUNOL 13, 255–263 (2012).
45. Rybtsov, S. *et al.* Tracing the origin of the HSC hierarchy reveals an SCF-dependent, IL-3-independent CD43(-) embryonic precursor. STEM CELL REP 3, 489–501 (2014).
46. Hovanessian, A.G. Midkine, a cytokine that inhibits HIV infection by binding to the cell surface expressed nucleolin. CELL RES 16, 174–181 (2006).
47. Said, E.A. *et al.* Pleiotrophin inhibits HIV infection by binding the cell surface-expressed nucleolin. FEBS J 272, 4646–4659 (2005).
48. Shibata, Y. *et al.* Nuclear targeting by the growth factor midkine. MOL CELL BIOL 22, 6788–6796 (2002).
49. Santos, T., Salgado, G.F., Cabrita, E.J. & Cruz, C. Nucleolin: a binding partner of G-quadruplex structures. TRENDS CELL BIOL 32, 561–564 (2022).
50. Mortensen, M. *et al.* The autophagy protein Atg7 is essential for hematopoietic stem cell maintenance. J EXP MED 208, 455–467 (2011).
51. Ho, T.T. *et al.* Autophagy maintains the metabolism and function of young and old stem cells. NATURE 543, 205–210 (2017).

52. Xi, Y. *et al.* Knockout of Atg5 delays the maturation and reduces the survival of adult-generated neurons in the hippocampus. CELL DEATH DIS 7, e2127 (2016).
53. Rudat, S. *et al.* RET-mediated autophagy suppression as targetable co-dependence in acute myeloid leukemia. LEUKEMIA 32, 2189–2202 (2018).
54. Stergiou, I.E. & Kapsogeorgou, E.K. Autophagy and Metabolism in Normal and Malignant Hematopoiesis. INT J MOL SCI 22 (2021).
55. Kuhn, K. & Romer, W. Considering autophagy, beta-Catenin and E-Cadherin as innovative therapy aspects in AML. *CELL DEATH DIS* 6, e1950 (2015).
56. Liu, Q., Chen, L., Atkinson, J.M., Claxton, D.F. & Wang, H.G. Atg5-dependent autophagy contributes to the development of acute myeloid leukemia in an MLL-AF9-driven mouse model. CELL DEATH DIS 7, e2361 (2016).
57. Warr, M.R. *et al.* FOXO3A directs a protective autophagy program in haematopoietic stem cells. NATURE 494, 323–327 (2013).
58. Ghaffari, S. Lysosomal Regulation of Metabolism in Quiescent Hematopoietic Stem Cells: More than Just Autophagy. CELL STEM CELL 28, 374–377 (2021).
59. Poillet-Perez, L., Sarry, J.E. & Joffre, C. Autophagy is a major metabolic regulator involved in cancer therapy resistance. CELL REP 36, 109528 (2021).
60. Mansell, E. *et al.* Mitochondrial Potentiation Ameliorates Age-Related Heterogeneity in Hematopoietic Stem Cell Function. CELL STEM CELL 28, 241–256 (2021).
61. Bennett, L.F., Mumau, M.D., Li, Y. & Speck, N.A. MyD88-dependent TLR signaling oppositely regulates hematopoietic progenitor and stem cell formation in the embryo. DEVELOPMENT 149 (2022).
62. Reglero-Real, N. *et al.* Autophagy modulates endothelial junctions to restrain neutrophil diapedesis during inflammation. IMMUNITY 54, 1989–2004 (2021).
63. Yu, Z. *et al.* Endothelial cell-derived angiopoietin-like protein 2 supports hematopoietic stem cell activities in bone marrow niches. BLOOD 139, 1529–1540 (2022).
64. Alva, J.A. *et al.* VE-Cadherin-Cre-recombinase transgenic mouse: a tool for lineage analysis and gene deletion in endothelial cells. Dev Dyn 235, 759–767 (2006).
65. Tsukamoto, S. *et al.* Autophagy is essential for preimplantation development of mouse embryos. SCIENCE 321, 117–120 (2008).
66. Janowska-Wieczorek, A. *et al.* Platelet-derived microparticles bind to hematopoietic stem/progenitor cells and enhance their engraftment. BLOOD 98, 3143–3149 (2001).
67. Li, Z. *et al.* Generation of hematopoietic stem cells from purified embryonic endothelial cells by a simple and efficient strategy. J GENET GENOMICS 40, 557–563 (2013).
68. McGinnis, C.S., Murrow, L.M. & Gartner, Z.J. DoubletFinder: Doublet Detection in Single-Cell RNA Sequencing Data Using Artificial Nearest Neighbors. CELL SYST 8, 329–337 (2019).
69. Hao, Y. *et al.* Integrated analysis of multimodal single-cell data. CELL 184, 3573–3587 (2021).

70. Subramanian, A. *et al.* Gene set enrichment analysis: a knowledge-based approach for interpreting genome-wide expression profiles. Proc Natl Acad Sci U S A 102, 15545–15550 (2005).
71. Macosko, E.Z. *et al.* Highly Parallel Genome-wide Expression Profiling of Individual Cells Using Nanoliter Droplets. CELL 161, 1202–1214 (2015).
72. Tirosh, I. *et al.* Dissecting the multicellular ecosystem of metastatic melanoma by single-cell RNA-seq. SCIENCE 352, 189–196 (2016).
73. Tirosh, I. *et al.* Single-cell RNA-seq supports a developmental hierarchy in human oligodendroglioma. NATURE 539, 309–313 (2016).
74. Qiu, X. *et al.* Reversed graph embedding resolves complex single-cell trajectories. NAT METHODS 14, 979–982 (2017).
75. La Manno, G. *et al.* RNA velocity of single cells. NATURE 560, 494–498 (2018).
76. Jin, S. *et al.* Inference and analysis of cell-cell communication using CellChat. NAT COMMUN 12, 1088 (2021).

Figures

Figure 1

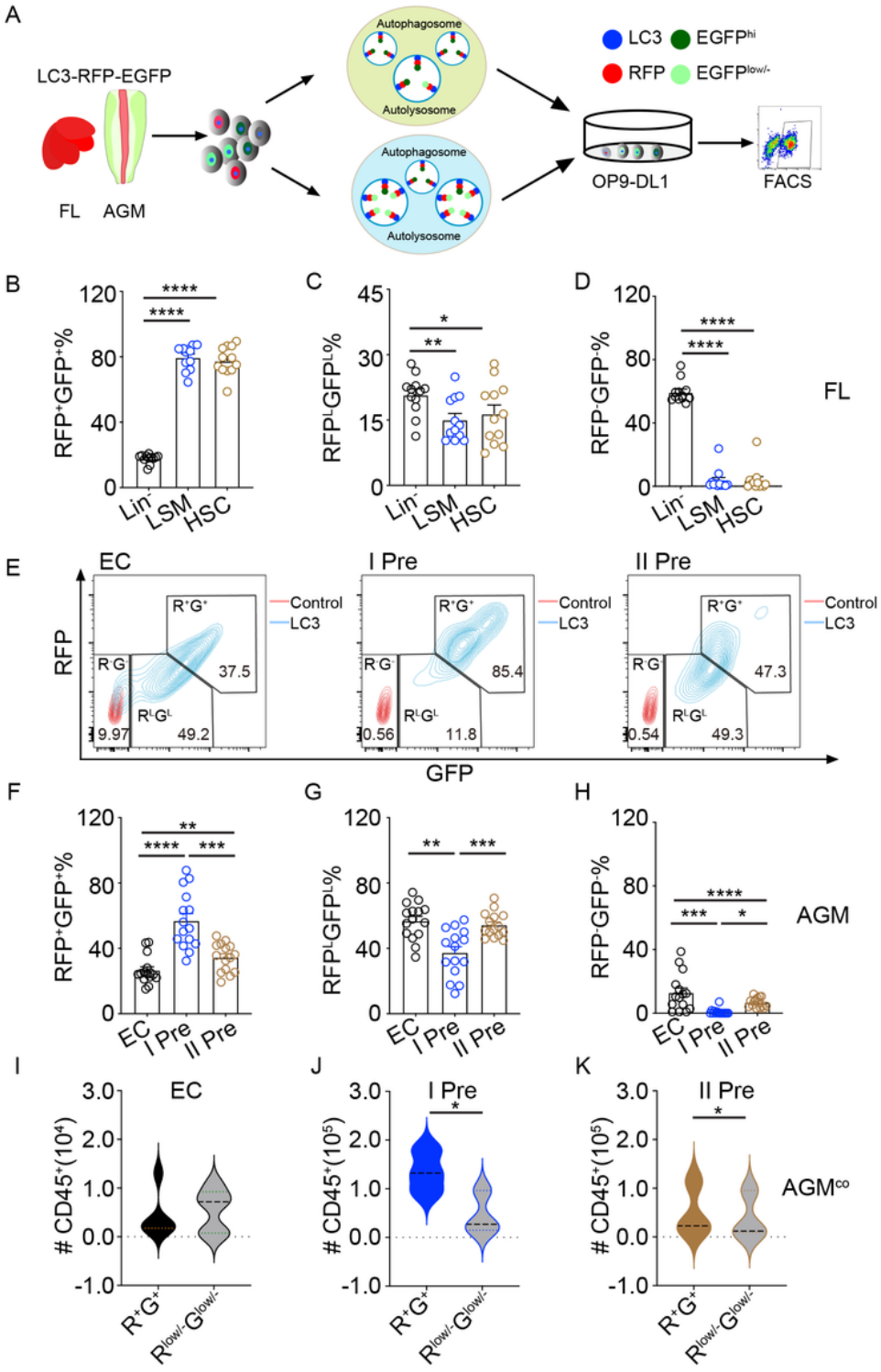

Figure 1

Identifying the autophagic status in E11.5 LC3-RFP-EGFP ($LC3^{R/G}$) AGM and E12.5 Fetal liver (FL) cells.

(A) The schematic for detecting autophagic status. (B-D) The percentage of RFP^+GFP^+ (B), $RFP^{low}GFP^{low}$ (C) and RFP^-GFP^- (D) in distinct cell fractions (Lin^-, LSM and HSC) of fetal liver. n=12, *p=0.042, **p=0.004, ****p<0.0001. (E) Presentative flow data displaying the RFP and GFP fluorescence level in

control viable cells and endothelial cells (EC, $CD31^{+}CD41^{-}CD45^{-}$), pre-HSC I (I Pre, $CD31^{+}CD41^{low}CD45^{-}$) and pre-HSC II (II Pre, $CD31^{+}CD45^{+}$) of E11.5 $LC3^{R/G}$ AGM region. WT viable cells as negative control. Red line=Control, blue line=$LC3^{R/G}$. (F-H) The percentage of $RFP^{+}GFP^{+}$ (F), $RFP^{low}GFP^{low}$ (G) and $RFP^{-}GFP^{-}$ (H) cells in distinct cell fractions of $LC3^{R/G}$ AGM region. n=15, *p=0.045, **p<0.01,***p<0.0001, ****p<0.0001. (I-K) The production of $CD45^{+}$ cells derived from both $RFP^{+}GFP^{+}$ and $RFP^{low/-}GFP^{low/-}$ subfractions in EC, I Pre, II Pre populations of $LC3^{R/G}$ AGM cocultured with OP9-DL1 (AGM^{co}). n≥3, *p<0.05.

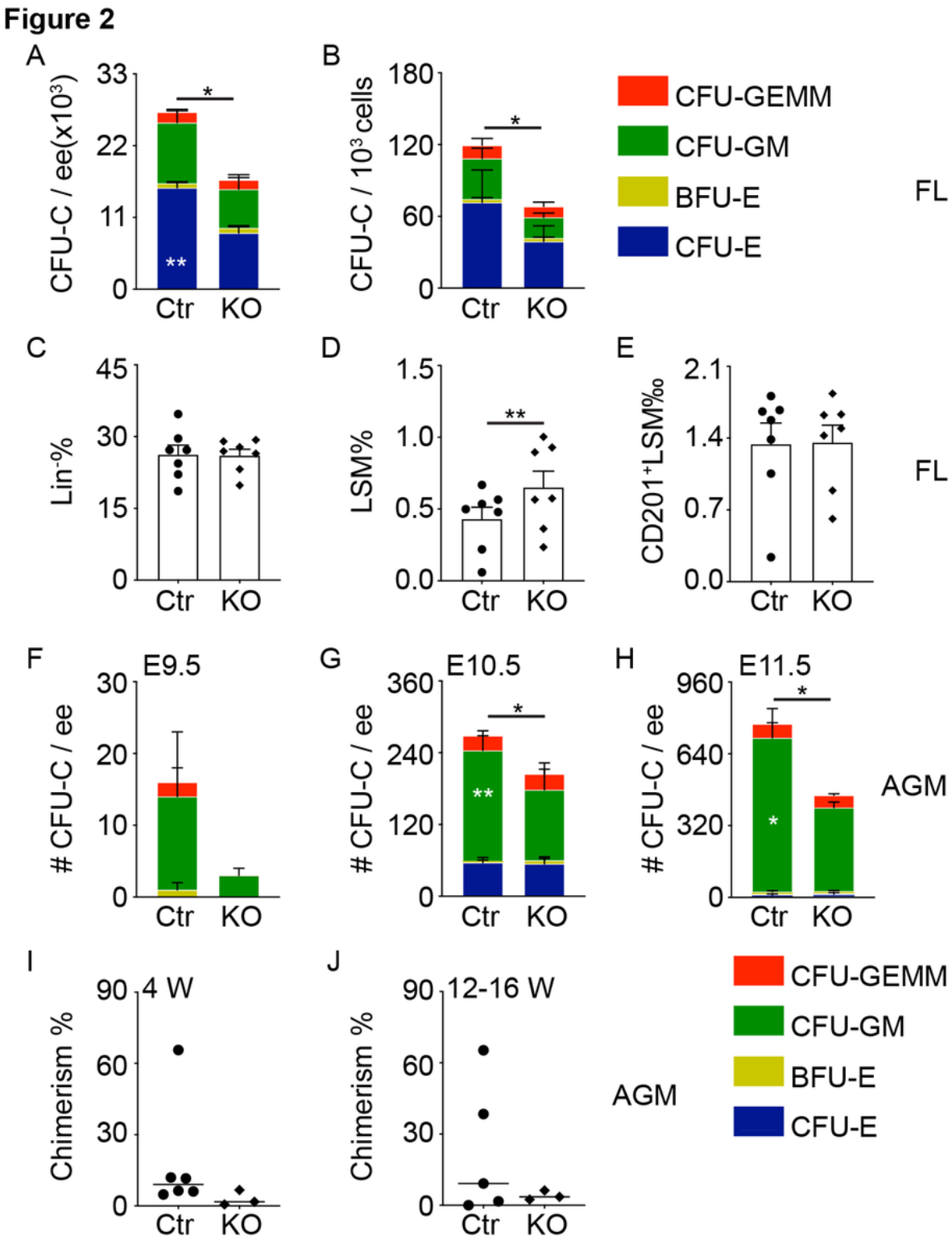

Figure 2

Atg5 deletion in endothelial cells leads to the reduction of hematopoietic progenitor cell and HSC. (A-B) Methylcellulose culture data showing the number of CFU-Cs and number of each hematopoietic colony type in the E12.5 fetal liver (indicated by color bars) per embryo equivalent (ee) or per 1000 input cells of control and KO. n=4, *p<0.05, **p<0.01. (C-E) Flow cytometric analysis showing the percentage of Lin^-, $Lin^-Sca1^+Mac1^{low}$ (LSM) and $CD201^+$LSM (HSC) in E12.5 fetal liver cells. n=7, **p=0.006. Circle=control (Ctr), inverted square=KO. (F-H) The number of CFU-Cs and number of each hematopoietic colony type in the E9.5-E11.5 AGM (indicated by color bars). n ≥3, *p<0.05, **p=0.0024. (I-J) Percentage of donor cell (CD45.2/2) chimerism in peripheral blood of irradiated recipients receiving control or KO AGM region cells after transplantation 4 weeks and 12-16 weeks. Circles and inverted squares indicate individual recipients of control or KO cells, respectively.

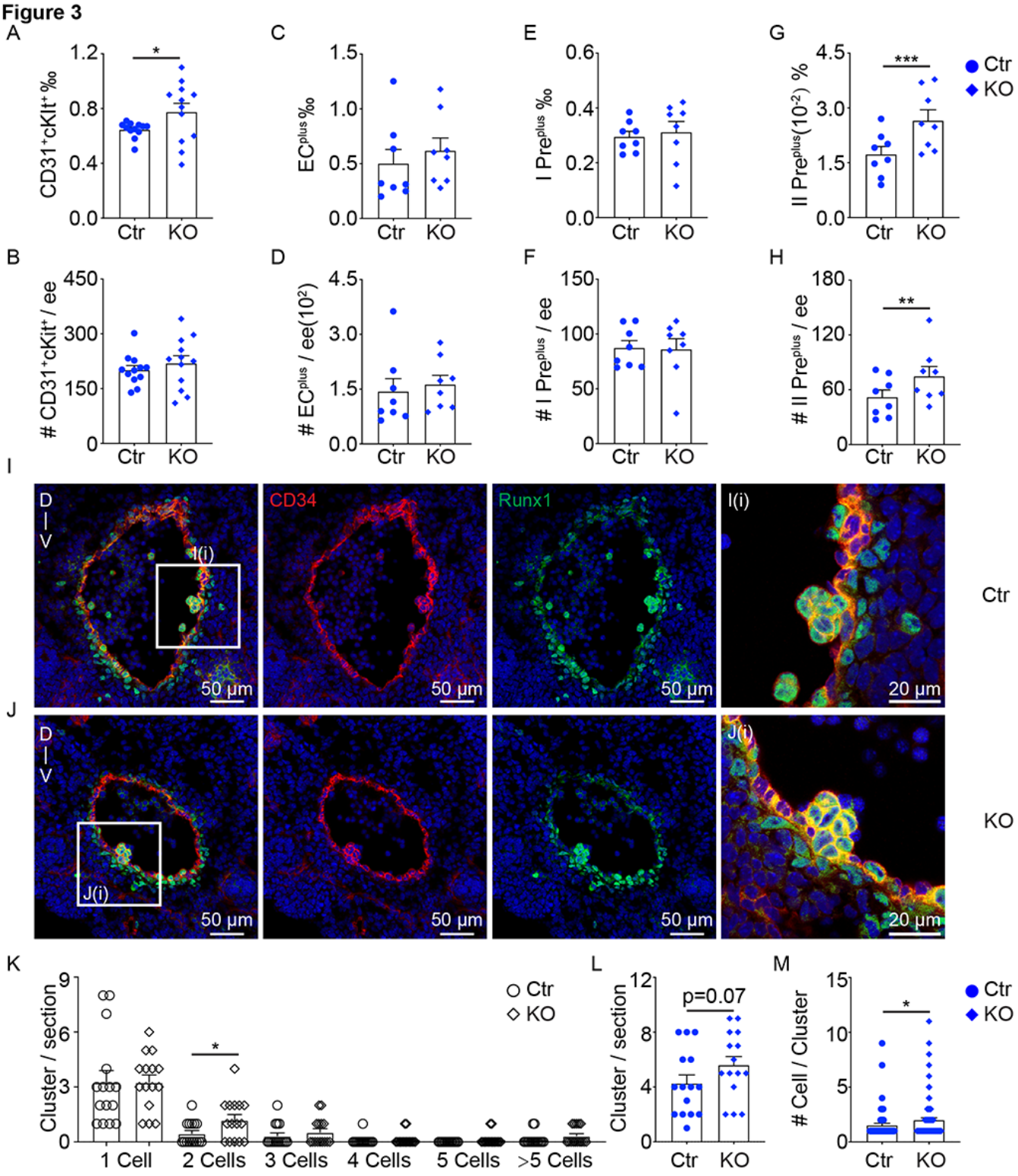

Figure 3

Immature hematopoietic precursor cells are increased after Atg5 ablation. (A-B) The percentage (A) of hematopoietic clusters ($CD31^+cKit^+$) was increased and the cell number (B) was comparable in the KO AGM as compared to control. n=12, *p=0.015. (C-H) The percentage (C, E and G) and cell number (D, F and H) of EC^{plus} ($CD31^+CD41^-CD45^-CD44^+CD201^+cKit^+DLL4^+$), pre-HSC I^{plus} ($I\ Pre^{plus}$, $CD31^+CD41^{low}CD45^-CD201^+\ cKit^+$) and pre-HSC II^{plus} ($II\ Pre^{plus}$, $CD31^+CD45^+CD201^+cKit^+$) in the E11.5

AGM region. n=8, **p=0.0036, ***p=0.0005. (I-J) Representative immunostaining of cryosections in E10.5 control (I) and KO (J) AGM region. Red=CD34, Blue=Hoechst, Green=Runx1. I (i) and J (i) showing the hematopoietic cluster cells in the control and KO aorta. Scale bars indicate in the figures. (K) Quantification of $CD34^{+}Runx1^{+}$ hematopoietic cluster cells using confocal images. Bars and symbols represent the number of clusters in each category of cluster cell size. Total 30 sections from 6 embryos were analyzed. n=3, *p=0.020. (L) The average number of $CD34^{+}Runx1^{+}$ hematopoietic clusters per section. n=3, p=0.070. (M) The average cell number in the detected $CD34^{+}Runx1^{+}$ hematopoietic clusters. n=3, *p=0.047. Circle=control (Ctr), inverted square=KO.

Figure 4

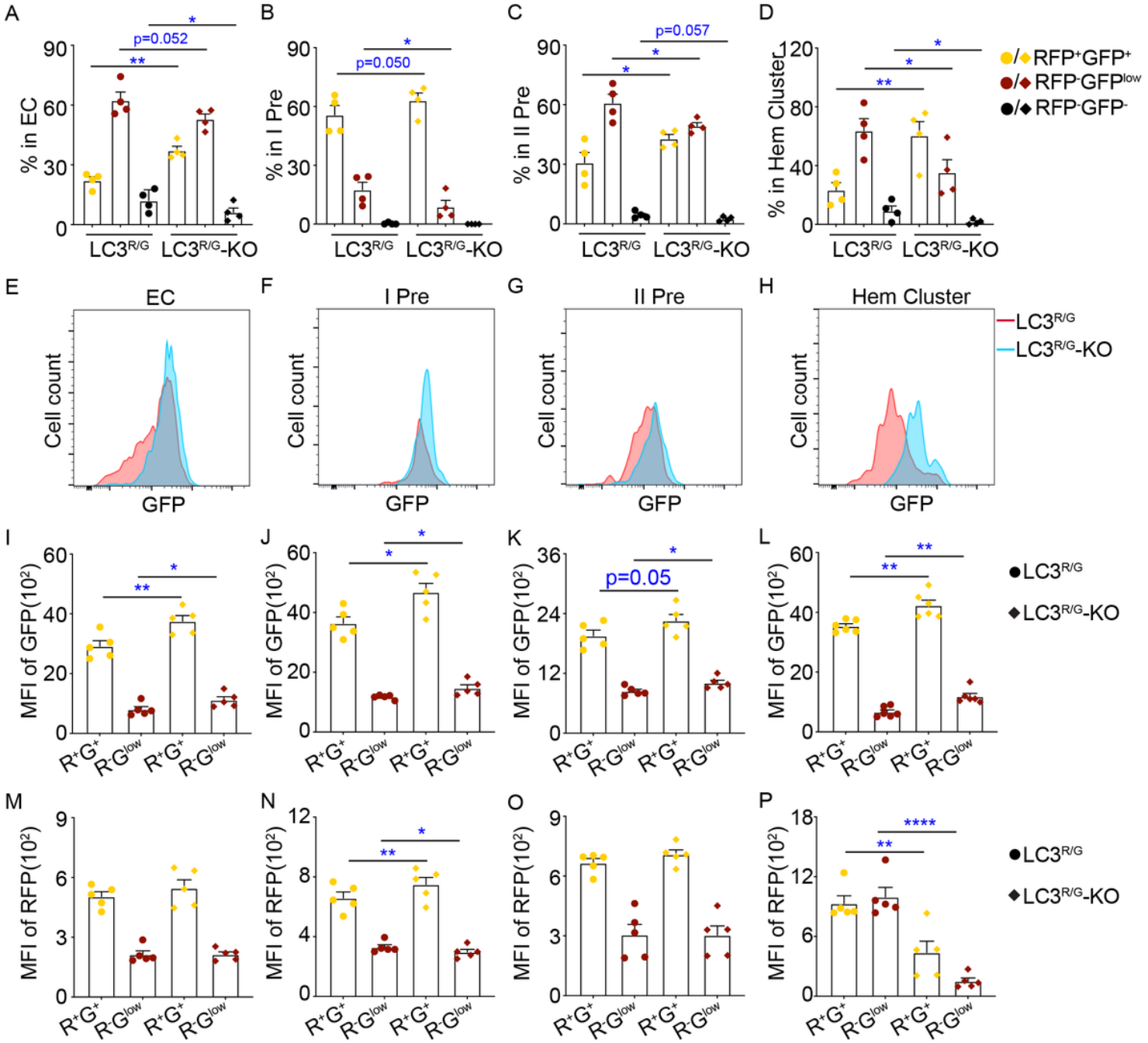

Figure 4

Atg5 deletion blocks the fusion between autophagosome and lysosome in E11.5 LC3-RFP-EGFP-Vec-Cre;Atg5$^{fl/fl}$ (LC3$^{R/G}$-KO) AGM cells. (A-C) Atg5 deficiency led to the increased percentage of RFP^{+}GFP^{+} cells and decreased the percentage of RFP^{low}GFP^{low} cells in the EC, pre-HSC I and pre-HSC II fractions. n=4, *p<0.05, ****p<0.0001. Colored circle=LC3$^{R/G}$, colored inverted square=LC3$^{R/G}$-KO. Yellow represents GFP^{+} signal and dark red represents GFP$^{low/-}$ signal. (D) The frequency of RFP^{+}GFP^{+}, RFP^{low}GFP^{low} and RFP^{-}GFP^{-} cells in the hematopoietic clusters from E11.5 LC3$^{R/G}$-KO AGM region. n=6, **p<0.01, ***p=0.0004. Hem cluster=hematopoietic clusters (CD31^{+}cKit^{+}). (E-H) Representative histogram showing the GFP fluorescence level in the EC, pre-HSC I, pre-HSC II and hematopoietic clusters. Red line=LC3$^{R/G}$ group, blue line= LC3$^{R/G}$-KO group. (I-L) Comparison analysis of the Geomean fluorescence intensity (GeoMFI) of GFP signals in the different fractions of EC, pre-HSC I, pre-HSC II and hematopoietic clusters of LC3$^{R/G}$ and LC3$^{R/G}$-KO. n=6, *p<0.05, **p<0.01. (M-P) The GeoMFI of RFP in the different fractions of EC, pre-HSC I, pre-HSC II and hematopoietic clusters of the LC3$^{R/G}$ and LC3$^{R/G}$-KO. n=6, *p=0.0218, **p<0.01, ****p=0.0000152. Circle= LC3$^{R/G}$, inverted square= LC3$^{R/G}$-KO.

Figure 5

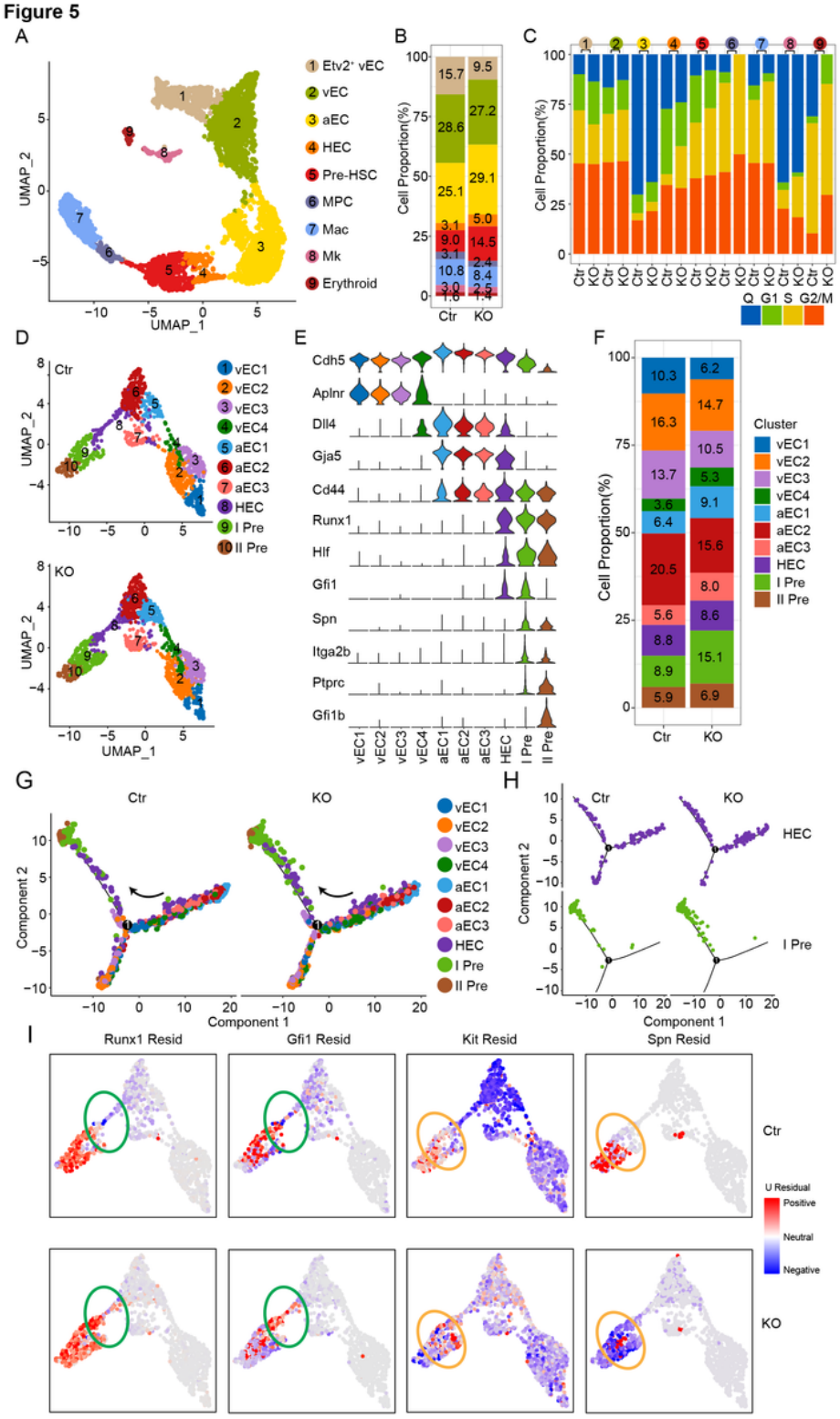

Figure 5

Comparative analysis by scRNA-Seq identifies cell components and developmental temporal order of hematopoietic related cells in the control and KO AGM region. (A). UMAP plots visualized nine clusters from hematopoietic related cells (EC, HC and Mk). (B) Bar graph showing the portions of each sub-cluster (EC and HC) in the control and KO AGM regions. (C) Bar charts showing the percentage contribution of different cell cycle phases in the control and KO cells. (D) UMAP plots visualized the ten clusters from

vEC, aEC, HEC and pre-HSCs. (E) Violin graphs displaying the key featured genes in each cell cluster. (F). Comparison analysis showing cell proportions of distinct clusters from EC and pre-HSCs between KO and control group. (G) Trajectory analysis by Monocle 2 indicating the alteration of developmental temporal order from EC to pre-HSCs. (H) Trajectory analysis showing the developmental temporal order of HEC and pre-HSC I (I Pre). (I) Comparative RNA velocyto analysis showed the status of unspliced and spliced genes in the control (Ctr) and KO group. Green circle labeled the HECs and Orange circle labels pre-HSC Is.

Figure 6

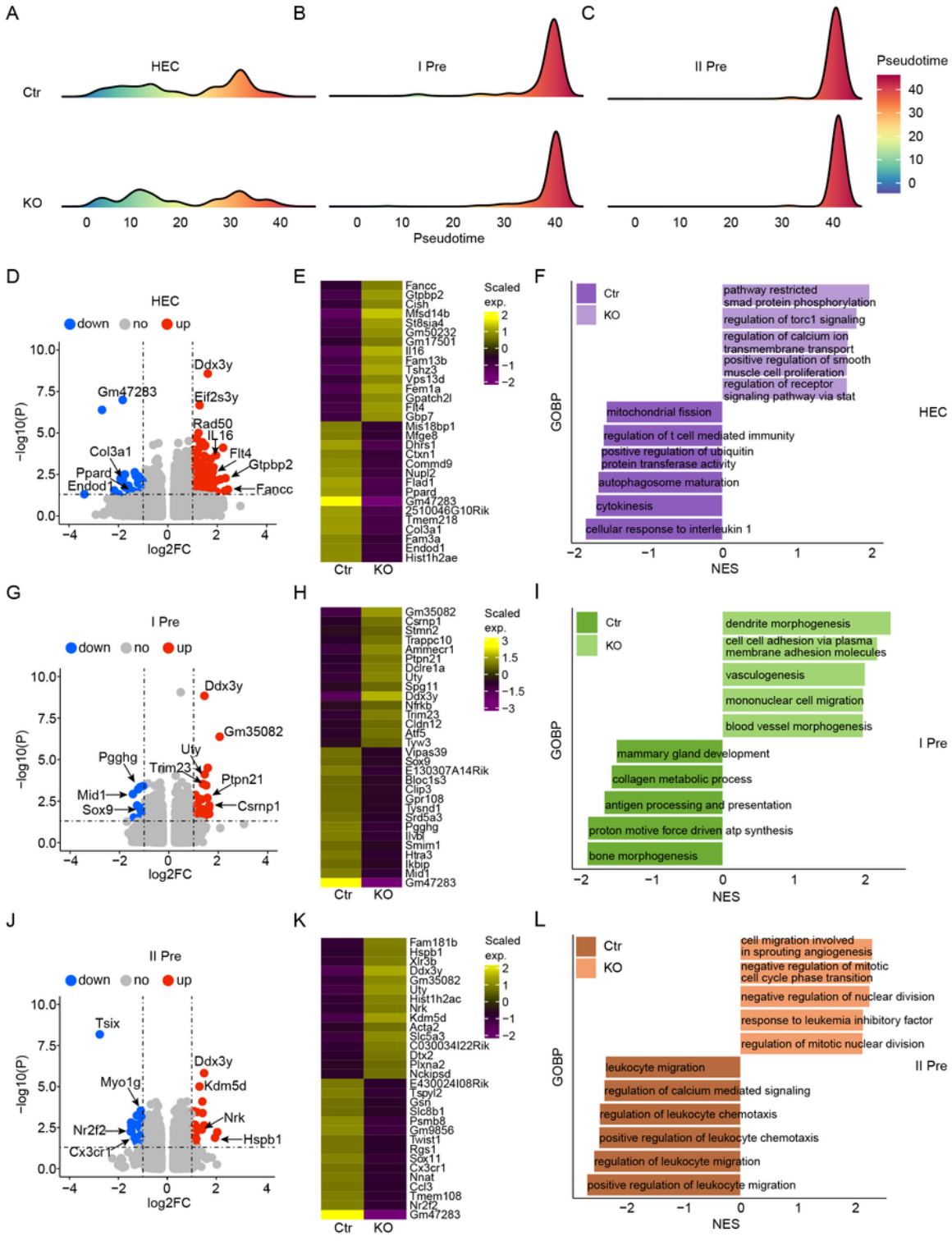

Figure 6

The differences in gene expression and biological process from HEC and pre-HSCs after Atg5 depletion. (A-C) The components of cell (HEC, pre-HSC I and pre-HSC II) in the indicated pseudotime by trajectory analysis. (D, G and J) Volcano graphs showing the up/down regulated genes in the KO HEC (D), pre-HSC I (G) and pre-HSC II (J) compared to control. Some up or down regulated genes were indicated. (E, H and K) Top 15 differentially expressed genes(DEGs) in the HEC (E), pre-HSC I (H) and pre-HSC II (K) compared KO with control group by scaled gene expression. (F, I and L) The enriched genes related with the biological processes are involved in the hematopoietic regulation and autophagy related process in the HEC (F), pre-HSC I (I) and pre-HSC II (L).

Figure 7

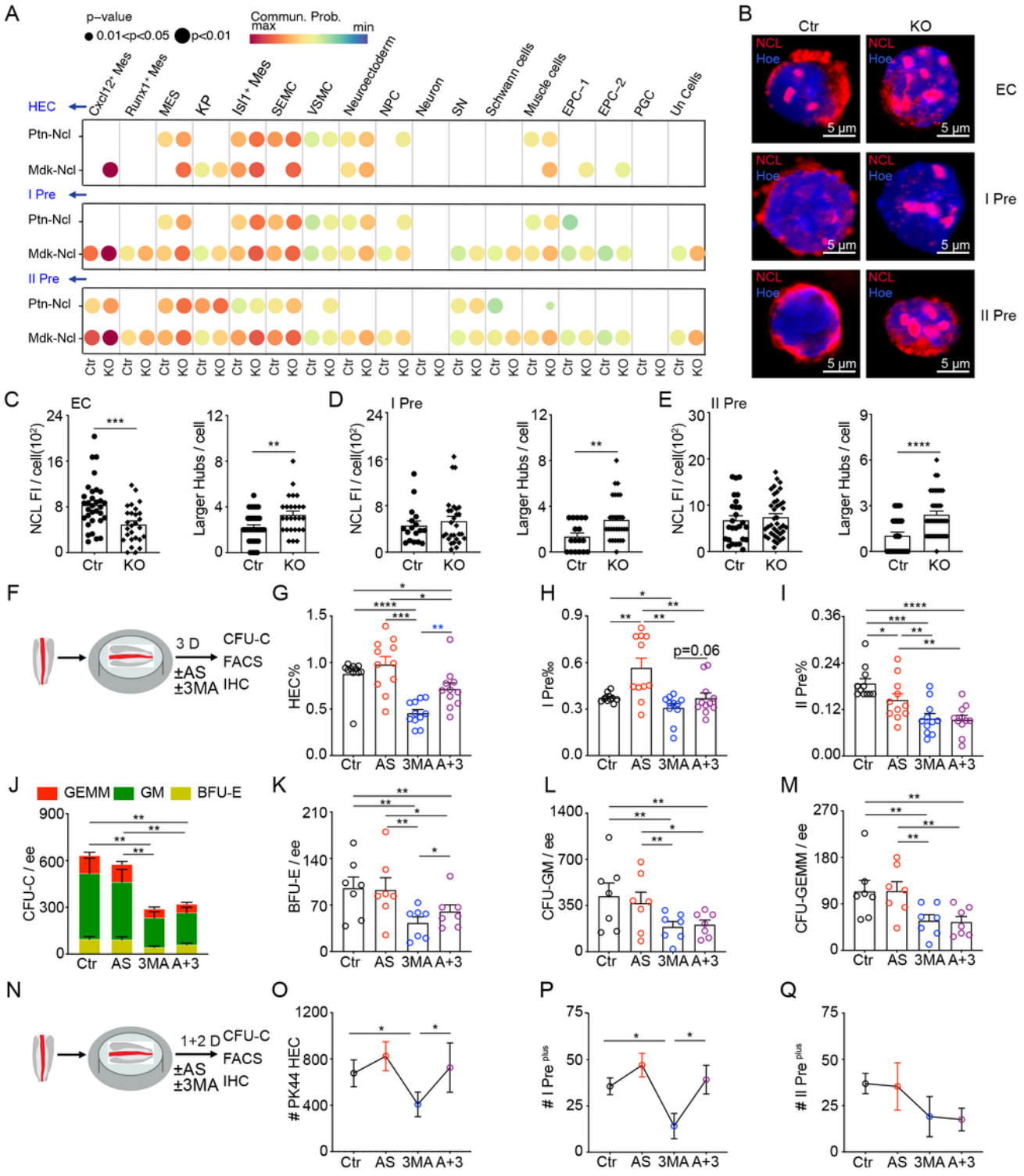

Figure 7

Atg5 regulates endothelial cell to hematopoietic transition through Ncl pathway. (A) Comparison analysis of the expression / interactions (Ptn-Ncl and Mdk-Ncl) between ligands from niche cells (excluding EC, pre-HSCs and Mk) and receptors from HEC, pre-HSC I and pre-HSC II in the control and KO group, showing the enhanced Ptn-Ncl and Mdk-Ncl interplays in these three fractions of KO group compared to control cells. (B) Representative immunostaining data of Ncl in the EC (up), pre-HSC I (I Pre, middle) and pre-HSC

II (II Pre, bottom) sorted from E10.5 control (Ctr) and KO AGM regions. Red=NCL, Blue=Hoe (Hoechst). (C-E) Fluorescence intensity (FI, left) in each cell fraction was calculated by image J and hubs (maximum length of each hub over one micrometer, right) of Ncl signal in the detected cells. n≥27 cells in EC, n≥17 in pre-HSC I, n≥26 in pre-HSC II. **p<0.001, ***p=0.0005, ****p<0.0001. (F) Experimental set-up for 3 days explant cultures. (G-I) 3 days E10.5 AGM explant cultures showing the rescue function in the percentages of HEC (G) after 3-MA and AS1411 treatment, but not in the pre-HSC I (H) and pre-HSC II (I) fractions. AS=AS1411, the aptamer of Ncl (also known as AGRO100). 3 MA=3-MA, the inhibitor of autophagy. A+3=AS1411+3 MA. n=11, *p<0.05, **p<0.01, ***p<0.001,****p<0.0001. (J) Total CFU-C number per AGM explant and number of each hematopoietic colony type (indicated by color bars) in the existence of AS1411 and 3-MA. (K-M) The number of BFU-E per AGM explant was increased in the AS1411+3-MA group compared to 3-MA group, but not in the CFU-GM and CFU-GEMM. n=7, *p<0.05, **p<0.01. (N) Experimental set-up for 1+2 days explant cultures. (O-Q) The number of PK44 ($CD31^{+}CD201^{+}cKit^{+}CD44^{+}CD45^{-}CD41^{-}$) and pre-HSC I^{plus} was rescued by AS1411 in the inhibition of 3-MA, but not in pre-HSC II^{plus}. n≥3, *p<0.05, **p<0.01.

Supplementary Files

This is a list of supplementary files associated with this preprint. Click to download.

- supLiuetalfiguresuplegends230822V1.pdf
- table.S2230822.xlsx
- tableS3230822.xlsx